IEEE Access
Multidisciplinary ⋮ Rapid Review ⋮ Open Access Journal

Received 7 September 2022, accepted 24 September 2022, date of publication 27 September 2022, date of current version 3 October 2022.

Digital Object Identifier 10.1109/ACCESS.2022.3210221

RESEARCH ARTICLE

Design and Test of a Curved-Beam Based Compliant Gripper for Manipulations of Actively Deformable Objects

QINGYI ZHANG[1], PENGBO LIU[2], (Member, IEEE), AND PENG YAN[1], (Senior Member, IEEE)

[1]Key Laboratory of High-Efficiency and Clean Mechanical Manufacture, Ministry of Education, School of Mechanical Engineering, Shandong University, Jinan, Shandong 250061, China

[2]School of Mechanical and Automotive Engineering, Qilu University of Technology (Shandong Academy of Sciences), Jinan 250353, China

Corresponding author: Peng Yan (yanpeng@sdu.edu.cn)

This work was supported in part by the Major Basic Research Program of the Natural Science Foundation of Shandong Province under Grant ZR2019ZD08, and in part by the National Natural Science Foundation of China under Grant 51905287.

ABSTRACT Sizes and stiffness variations of actively deformable objects pose significant challenges on the design of compliant constant-force gripper. This paper presents a curved-beam based constant force compliant gripper which is composed of the constant force module, the bistable module, the preloading module and the linear guide. A curved-beam constant force mechanism is designed to generate constant force output, the non-constant force motion range of which is further eliminated via curved-based bistable mechanism and preloading module. After a formulation to find the optimal gripper configuration, the design is verified through comparison with simulation results. Finally, a prototype of the proposed gripper is tested to demonstrate its grasping capacity.

INDEX TERMS Compliant gripper, constant force mechanism, force-sensitive manipulation, actively deformable object.

I. INTRODUCTION

Force-sensitive manipulation has emerged as one of the key enabling technologies in many advanced engineering areas such as robotic surgical devices [1], [2] and cell microinjection [3]. Maintaining a proper grasping force is a significant concern during the manipulating process [4], [5]. In particular, actively deformable objects, such as animals, living organs (heart, blood vessels), pose significant challenges on the design of compliant grippers with large operating ranges and adjustable jaw clearance [6]. Compliant grippers equipped with force and displacement sensors are usually utilized to minimize the possibility of damaging the objects, resulting in higher cost and system complexity [7], [8], [9].

Compliant constant force grippers can deliver precise force output independent on complex control algorithms and structures [10] and thus are perfect candidates for handling and manipulating delicate objects with various sizes and stiffness [11], [12]. Grippers based on constant force mechanisms have been developed, where representative results include two-stage microgripper [13], bi-directionally adjustable gripper [14], force-sensing microinjector [15], apple picking actuator [16], 3D-printed gripper [17], 2-DOF gripper [18], [19], multi-mode gripper [20], [21].

A major issue for manipulating actively deformable objects is the sizes and stiffness variations. Proper grasping force is necessary for safe grasping in its deformation range. However, the nonlinear deformation behavior of thin leaf beam results in a relatively small stroke and additional challenges on manufacturability and cost [15]. Due to manufacturing errors, prototypes of well-designed constant force mechanism are prone to negative stiffness characteristics in its large deformation, which is detrimental to the reliability of force-sensitive manipulation [17]. In addition, the clearance of the

The associate editor coordinating the review of this manuscript and approving it for publication was Jingang Jiang.

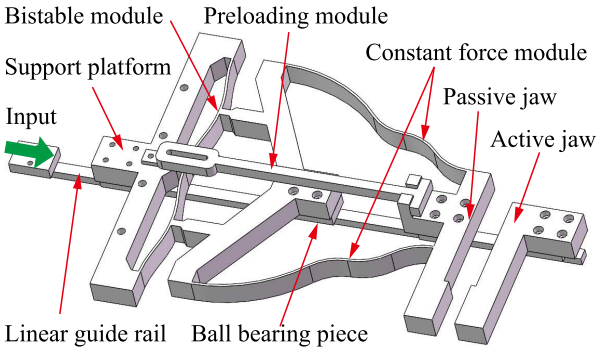

FIGURE 1. Schematic diagram of the constant force compliant gripper.

jaws is often not adjustable. As a result, the grasping capacity remains limited within a small range [22], [23].

This paper presents a curved-beam based constant force compliant gripper for grasping actively deformable objects, which is configurable with appropriate arc-elements to achieve constant force output with a large motion stroke. A curved-based bistable mechanism is fused to eliminate the non-constant force motion range of the constant force mechanism. The rest of this paper is organized as follows. The design concept, working principle of the proposed gripper are introduced in Section II. An analytical modeling is derived in Section III. Parameter optimization and simulation verification are conducted in Section IV. In Section V, the mechanism prototype is manufactured and tested. Finally, some concluding remarks are made in Section VI.

II. MECHANISM DESIGN

The mechanical structure of the developed compliant gripper is illustrated in Figure 1. The proposed gripper consists of a pair of jaws, a constant force module (CFM), a bistable module (BM), a preloading module and a linear guide module. Considering the compactness, the jaws compose of a passive constant-force jaw and an active jaw. A four-arc curved-beam based compliant constant structure is employed in this gripper to obtain constant gripping force output [24]. Note that preshaped bistable beams with both ends fixed are widely used because they are easy to fabricate and do not require external forces or hinged boundaries to induce buckling [25]. To facilitate fabrication and analysis of the gripper, we select a curved-beam based compliant mechanism as the bistable structure, which is connected with the CFM and the left jaw in series. The preloading module fixed on the BM is connected with the right end of the CFM to eliminate the non-constant force motion range of the CFM. The right jaw, the CFM and the BM are connected with linear guide rail via ball bearing piece to constrain the degrees of freedom in other directions. Considering the large working stroke, direct drive units, such as voice coil motors, can be used to drive the gripper.

The working principle of the developed gripper is described in Figure 2. The configuration of the gripper and the corresponding force-displacement curve are shown in Figure 2(a). F_{obj}, S_{obj}, κ_{obj} is the desired constant force, motion range and the stiffness of the gripper, respectively. S_1, S_2, κ_1, κ_2 are the stroke and stiffness of non-constant and constant force stage of CFM, respectively. As shown in Figure 2(b), a_1 is the distance between CFM and BM, which can be set via the preloading module. a_2 is the stroke of the BM between its two steady states.

When no preloading is applied to the constant force mechanism, the BM is in the left stable state position. There is a slow force growth process (AB) before entering the constant force stage (BC), which usually indicates low gripping efficiency. When the BM is in the right stable state position, a preloading displacement a_2 ($\geq$ S_1) is applied to the constant force mechanism, the gripper generate constant force output immediately when displacement is applied. Fix the BM and apply displacement to the linear guide rail, the jaw moves along linear guide, accompanied by a nearly constant force output over a large range. An expected constant gripping force can then be obtained by optimizing the structure parameters.

III. MODELING OF THE GRIPPER

In order to obtain the gripper with expected force output, it is necessary to appropriately configure the bistable behavior of the bistable module (BM) and the constant force property of the constant force module (CFM). For this purpose, the theoretical models are established to predict the force-displacement relationships of the BM and CFM, respectively.

A. FORCE-DISPLACEMENT EQUATIONS OF CURVE BEAM

The kinetostatic model of the gripper is derived by Chained Beam Constraint Model (CBCM) [26]. The load–deflection equations are recalled as follows [27]:

$$\begin{cases} \begin{bmatrix} f_i \\ m_i \end{bmatrix} = \begin{bmatrix} 12 & -6 \\ -6 & 4 \end{bmatrix} \begin{bmatrix} \delta_i \\ \alpha_i \end{bmatrix} \\ \quad + p_i \begin{bmatrix} 6/5 & -1/10 \\ -1/10 & 2/15 \end{bmatrix} \begin{bmatrix} \delta_i \\ \alpha_i \end{bmatrix} \\ \quad + p_i^2 \begin{bmatrix} -1/700 & 1/1400 \\ 1/1400 & -11/6300 \end{bmatrix} \begin{bmatrix} \delta_i \\ \alpha_i \end{bmatrix} \\ \quad + p_i \begin{bmatrix} \kappa_i/2 \\ \kappa_i/12 \end{bmatrix}, \\ \lambda_i = \dfrac{t_i^2 p_i}{12} - \dfrac{\kappa_i}{2}\delta_i - \dfrac{\kappa_i}{12}\alpha_i \\ \quad - \dfrac{1}{2} \begin{bmatrix} \delta_i & \alpha_i \end{bmatrix} \begin{bmatrix} 6/5 & -1/10 \\ -1/10 & 2/15 \end{bmatrix} \begin{bmatrix} \delta_i \\ \alpha_i \end{bmatrix} \\ \quad - p_i \begin{bmatrix} \delta_i & \alpha_i \end{bmatrix} \begin{bmatrix} -1/700 & 1/1400 \\ 1/1400 & -11/6300 \end{bmatrix} \begin{bmatrix} \delta_i \\ \alpha_i \end{bmatrix} \\ \quad + p_i \dfrac{\kappa_i}{360}\alpha_i + p_i \dfrac{\kappa_i^2}{720}, \end{cases} \tag{1}$$

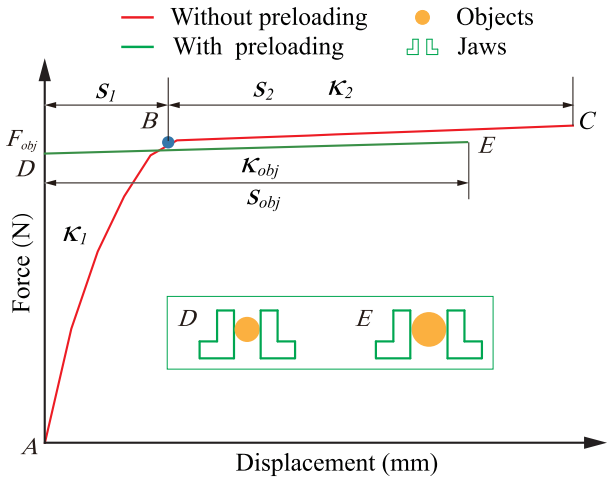

(a) Force-displacement curve

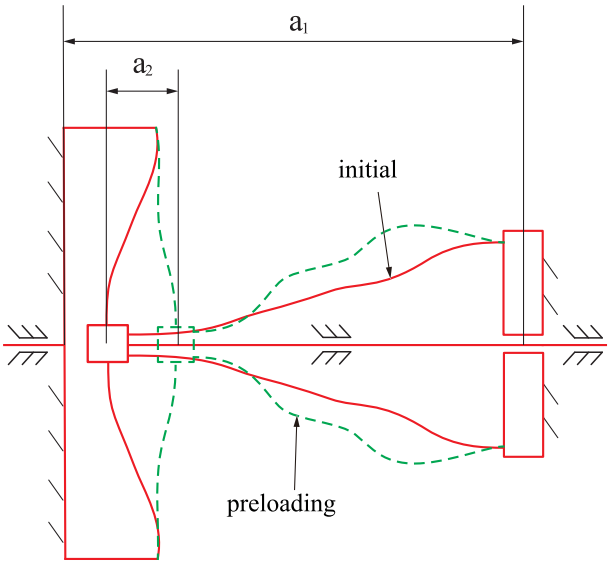

(b) Configuration of curved beams

FIGURE 2. Working principle of the compliant gripper.

where all the parameters are normalized with respect to the dimensions L_i of an element as

$$\begin{cases} p_i = \dfrac{P_i L_i^2}{EI}, \\ f_i = \dfrac{F_i L_i^2}{EI}, \\ m_i = \dfrac{M_i L_i}{EI}, \\ t_i = \dfrac{T_i}{L_i}, \\ \kappa_i = K_i L_i, \\ \lambda_i = \dfrac{\Lambda_i}{L_i}, \\ \delta_i = \dfrac{\Delta_i}{L_i}, \\ \alpha_i = \alpha_i, \end{cases} \tag{2}$$

where P_i, F_i, M_i, Λ_i, Δ_i, T_i, K_i are axial force, transverse force, moment, axial deflections, transverse deflections, beam thickness and curvature, respectively. $p_i, f_i, m_i, \lambda_i, \delta_i, t_i, k_i$ are the corresponding normalized parameters, respectively. α_i is the end slope. L_i is the nominal length of each element and can be calculated as

$$L_i = L_{xi} \cos \beta_i + L_{yi} \sin \beta_i, \tag{3}$$

where β_i is the end slope of node i, and L_{xi} and L_{xi} are the length components of each element along x- and y-axis. They can be calculated by

$$\begin{cases} L_{xi} = x_{i+1} - x_i, \\ L_{yi} = y_{i+1} - y_i, \end{cases} \tag{4}$$

where (x_i, y_i) and (x_{i+1}, y_{i+1}) are the coordinates of node i and node $i+1$, respectively.

The static equilibrium equations between the i-th and first element can be expressed as [28]

$$\begin{bmatrix} \cos\varphi_i & \sin\varphi_i & 0 \\ -\sin\varphi_i & \cos\varphi_i & 0 \\ (1+\lambda_i) & -(0.5\kappa_i + \delta_i) & 1 \end{bmatrix} \begin{bmatrix} f_i \\ p_i \\ m_i \end{bmatrix} = \begin{bmatrix} \dfrac{f_1 L_i^2}{L_1^2} \\ \dfrac{p_1 L_i^2}{L_1^2} \\ \dfrac{m_{i-1} L_i}{L_{i-1}} \end{bmatrix}, \tag{5}$$

$$\begin{cases} P_o = P_1 = \dfrac{p_1 EI}{L_1^2}, \\ F_o = F_1 = \dfrac{f_1 EI}{L_1^2}, \\ M_o = M_N = \dfrac{m_N EI}{L_N}. \end{cases} \tag{6}$$

where E and I are Young's modulus and moment of inertia, respectively.

The geometric constraint equations are recalled as [28]

$$\begin{cases} \sum_{i=1}^{N} \left[(1+\lambda_i) L_i \cos\theta_i - (0.5\kappa_i + \delta_i) L_i \sin\theta_i \right] = X_o \\ \sum_{i=1}^{N} \left[(1+\lambda_i) L_i \sin\theta_i + (0.5\kappa_i + \delta_i) L_i \cos\theta_i \right] = Y_o \\ \beta_{N+1} + \sum_{i=1}^{N} \alpha_i = \theta_o \end{cases} \tag{7}$$

where θ_i is the rotation angle of i-th element's coordinate frame to the global coordinate frame that can be directly expressed by

$$\begin{cases} \theta_1 = 0, \\ \theta_i = \beta_i + \sum_{k=1}^{i-1} \alpha_k (i = 2, 3, \ldots, N). \end{cases} \tag{8}$$

Equations (1) - (8) form the governing equations of CBCM. By simultaneously solving them, the kinetostatic behaviors of the beam can be obtained.

B. MODELING OF CFM

Considering the symmetry, a half of the mechanism was chosen to derive an analytical model based on chained beam constraint model (CBCM) as shown in Figure 3. To facilitate the calculation, the starting point of the curved-beam coincides with the origin O of the coordinate system. Radial force F_{o1}, tangential force P_{o1} and moment M_{o1} are applied at the right end, receptively.

The multi-sectional circular curved-beam is determined by ten design parameters, namely, φ_i, R_i ($i \in \{1, 2, 3, 4\}$), T_1, W_1, where R_i and φ_i is radius and central angle of each segment, T_1 and W_1 are the in-plane and out-of-plane thickness, respectively. The adjacent segments are tangent at the intersections. To facilitate manufacturing and modeling, the thickness T_1 and W_1 are assumed to be uniform along the direction of the curved-beam.

Geometric equations of the multi-sectional circular curved-beam is first derived. According to the parametric equation of the circular arc, the coordinates of point (x_n, y_n) on the n-th ($n \in \{1, 2, 3, 4\}$) arc can be expressed as [24]

$$\begin{cases} x_n = Xo_n + R_n cos(t_n), \\ y_n = Yo_n + R_n sin(t_n), \end{cases} \tag{9}$$

where Xo_n, Yo_n, R_n are center coordinate and radius of the n-th arc, respectively. In (9), Xo_n, Yo_n and t_n can be deduced from the curve shape. Geometric relationship of center coordinates between neighboring arcs can be calculated from the central angle φ_i and radius R_i of the circular arc by using the following equations

$$\begin{cases} Xo_1 = Xo_0, \\ Yo_1 = Yo_0, \\ Xo_2 = Xo_1 + (R_1 + R_2)\cos(\varphi_1), \\ Yo_2 = Yo_1 - (R_1 + R_2)\sin(\varphi_1), \\ Xo_3 = Xo_2 - (R_2 + R_3)\cos(\varphi_1 - \varphi_2), \\ Yo_3 = Yo_2 + (R_2 + R_3)\sin(\varphi_1 - \varphi_2), \\ Xo_4 = Xo_3 + (R_3 + R_4)\cos(\varphi_1 - \varphi_2 + \varphi_3), \\ Yo_4 = Yo_3 - (R_3 + R_4)\sin(\varphi_1 - \varphi_2 + \varphi_3), \end{cases} \tag{10}$$

where the range of parameter t_n can be obtained by

$$\begin{cases} t_1 = (0, \varphi_1), \\ t_2 = (\varphi_1 + \pi, \varphi_1 + \pi - \varphi_2), \\ t_3 = (\varphi_1 + 2\pi, \varphi_1 + 2\pi + \varphi_3), \\ t_4 = (\varphi_1 + 3\pi + \varphi_3, \varphi_1 + 3\pi + \varphi_3 - \varphi_4). \end{cases} \tag{11}$$

Assume that the j-th circular arc is divided into n_j elements with equal central angle $t_u = \min(\varphi_j/n_j)$. The discrete parameter t_i can be obtained by dividing t_n with interval t_u. The discrete curve coordinates at the corresponding discrete points $(x_{1,i}, y_{1,i})$ can be calculated by recalling (9) - (11). The slope $\beta_{1,i}$ and curvature $K_{1,i}$ of the curve at discrete points $(x_{1,i}, y_{1,i})$ are then obtained by

$$\beta_{1,i} = \arctan \frac{1}{tan(t_i)}, \tag{12}$$

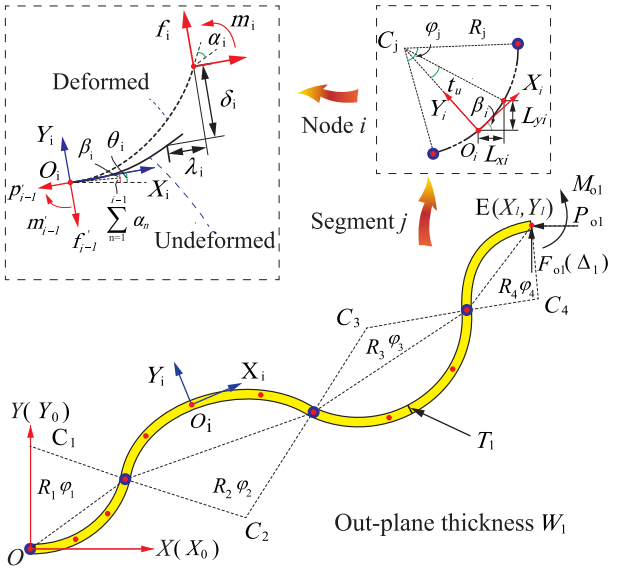

FIGURE 3. The schematic diagram of the CFM.

and

$$K_{1,i} = \frac{sin^2(t_i) - cos^2(t_i)}{(\frac{1}{tan(t_i)})^3 sin^3(t_i)}. \tag{13}$$

For a given displacement Δ_1 in global coordinate system, the corresponding tip coordinates and tip slope can be expressed as follows according to external geometric constraints

$$\begin{cases} X_{o1} = X_1 - \Delta_1, \\ Y_{o1} = Y_1, \\ \theta_{o1} = 0, \end{cases} \tag{14}$$

where X_1, Y_1 are calculated by (9) - (10). Then P_{o1} and F_{o1} can be obtained by solving (1) - (8) with *fsolve* function in MATLAB. The force required to actuate the CFM is calculated by

$$F_{cfm} = -2\, P_{o1}. \tag{15}$$

C. MODELING OF BM

Figure 4 shows the illustration of the unit cell of the bistable mechanism. The unit cell can be simplified into a cosine-shaped beam and some stiffening walls. The parameters that determined the layout of the cosine-shaped beam are marked in Figure 4, where T_2, W_2, H, and L_2 are the thickness, width, height, and span of the cosine-shaped beam, respectively.

The configuration of the neutral axis of the curved beam can be predicted by [29]

$$y = \frac{H}{2}\left[1 + \cos\left(\frac{2\pi x}{L_2}\right)\right] + \frac{T_2}{2}, \quad x \in [0, L_2] \tag{16}$$

For the noncircular beam, it is convenient to divide the beam into N_2 elements at nodes O_i along X-axis with approximately

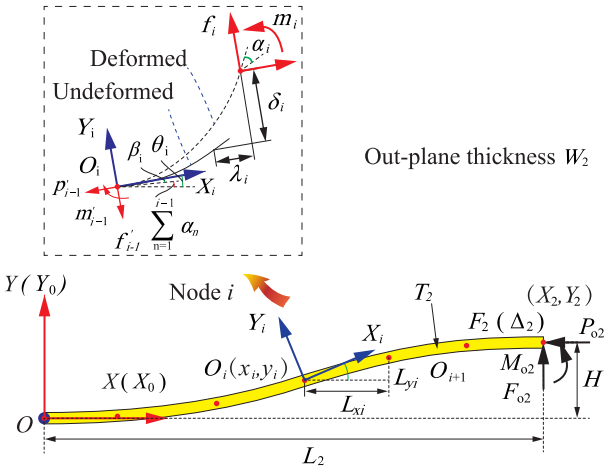

FIGURE 4. The schematic diagram of the BM.

equal lengths [28]. The coordinates of node i is

$$x_{2,i} = i\frac{L_2}{N_2}, \quad i \in [0, N_2] \tag{17}$$

and the corresponding coordinates along the Y-axis is

$$y_{2,i} = \frac{H}{2}\left[1 + \cos\left(\frac{2\pi x_{2,i}}{L_2}\right)\right] + \frac{T_2}{2}, \quad x \in [0, L_2] \tag{18}$$

The slope $\beta_{2,i}$ and curvature $K_{2,i}$ of the curve at discrete points $(x_{2,i}, y_{2,i})$ are then obtained by

$$\beta_{2,i} = \arctan(-\frac{2\pi H}{L_2} sin(\frac{2\pi x_{2,i}}{L_2})) \tag{19}$$

and

$$K_{2,i} = \frac{\frac{4\pi^2 H}{L_2{}^2} cos(\frac{2\pi x_{2,i}}{L_2})}{(1 + \frac{4\pi^2 H^2}{L_2{}^2} sin^2(\frac{2\pi x_i}{L_2}))^{\frac{3}{2}}}. \tag{20}$$

For a given displacement Δ_2 in global coordinate system, the corresponding tip coordinates and tip slope can be expressed as follows according to external geometric constraints

$$\begin{cases} X_{o2} = X_2, \\ Y_{o2} = Y_2 - \Delta_2, \\ \theta_{o2} = 0, \end{cases} \tag{21}$$

where X_2, Y_2 are calculated by (17) - (18). Then P_{o2} and F_{o2} can also be obtained by solving (1) - (8) with *fsolve* function in MATLAB. The force required to actuate the BM is

$$F_{bm} = -4\, F_{o2}. \tag{22}$$

For the whole gripper, the input displacement of jaw Δ, the displacement of CFM Δ_1, the displacement of BM Δ_2, and corresponding force satisfy the following constraints

$$\begin{cases} \Delta = \Delta_1 + \Delta_2, \\ F = F_{cfm} - \mu M = F_{bm} - \mu M. \end{cases} \tag{23}$$

where μ and M are the friction coefficient of the linear guide and the mass of the objects, respectively.

The force-displacement characteristics of the gripper can be obtained by giving different input displacements Δ. The desired output force F_{obj} (Figure 2(a)) is expressed as

$$F_{obj} = \frac{F_B + F_C}{2}, \tag{24}$$

where F_B and F_C are output forces at point B and C, respectively. The position of point B is specified according to the desired constant force range S_{obj}. The desired stiffness in the second stage κ_2 (≥ 0) is expressed as

$$\kappa_{obj} = \frac{F_C - F_B}{S_2}, \tag{25}$$

where S_1 and S_2 are the stroke in the first stage and the stroke in the second stage of the CFM, respectively.

IV. PARAMETER OPTIMIZATION AND SIMULATION VERIFICATION

A. PARAMETERS OPTIMIZATION

On the basis of the established kinetostatic model, parameter optimization of the proposed gripper is conducted in this section. To obtain constant output force, a specific output force and small positive stiffness are expected at the same time. Hence, a multiobjective optimization problem are specified by

$$\begin{aligned} \min & \begin{bmatrix} F_{obj}(R_1, R_2, R_3, L_2) \\ \kappa_{obj}(R_1, R_2, R_3, L_2) \end{bmatrix} \\ \text{s.t. } & R_{\min} \leq R_i \leq R_{\max}, \quad i = 1, 2, 3, \\ & L_{2,\min} \leq L_2 \leq L_{2,\max}. \end{aligned} \tag{26}$$

Set the goal [8, 0.005] and weight [0.001, 0.003], and solve the goal attainment problem starting at [30, 30, 90, 20]. To make the objective function as near as possible to a goal value (that is, neither greater than nor less than), the 'EqualityGoalCount' option is set to 2. The in-plane thickness T_1 and T_2 are set to 1 mm to facilitate additive manufacturing. To obtain bistable response, it is suggested that $H/T_2 \geq 3.33$ [29]. In addition, it is also suggested that $2H \geq S_2$ to switch working mode. Hence, H is set to 4 mm. The polymeric material nylon (Young's modulus E = 2320 MPa, Poisson's ratio $\mu = 0.394$ and yield strength S_y = 46 MPa) is considered as the material in view of additive manufacturing of the developed gripper. The radius R_i is set to 10 mm-90 mm and φ_i is set to 45°. By multiobjective goal attainment method, an optimized grasping forces of 8.06 N is obtained with the parameters listed in Table 1.

B. SIMULATION VERIFICATION

On top of the optimization results, the mechanical performance of the CFM and BM is validated by finite element analysis (FEA) through the software ANSYS.

The constant force characteristics of the CFM is first investigated. As illustrated in Figure 5, the CFM produce a near constant output force of 8.06 N in a large range of 18 mm,

TABLE 1. Key structure parameters of the compliant gripper.

Parameter	Value	Parameter	Value
φ_i	45 °	R_3	22.46 mm
R_1	61.21 mm	R_4	22.46 mm
R_2	20.33 mm	T_1	1 mm
T_2	1 mm	H	4 mm
L_2	29.95 mm	W_1	10 mm
W_2	10 mm		

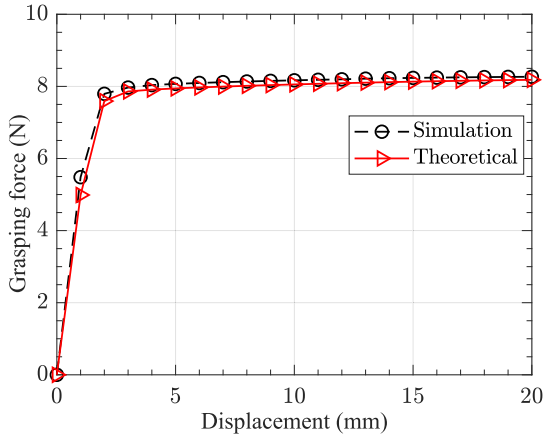

(a) Force-displacement curve

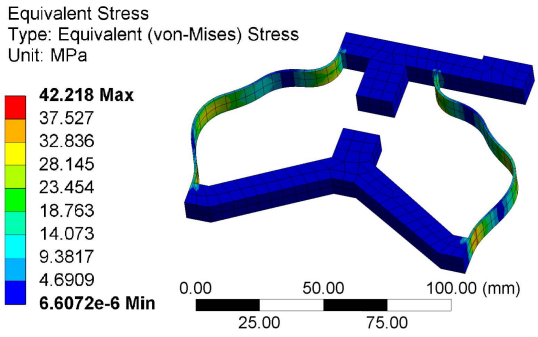

(b) Stress distribution

FIGURE 5. Simulation verification of the CFM.

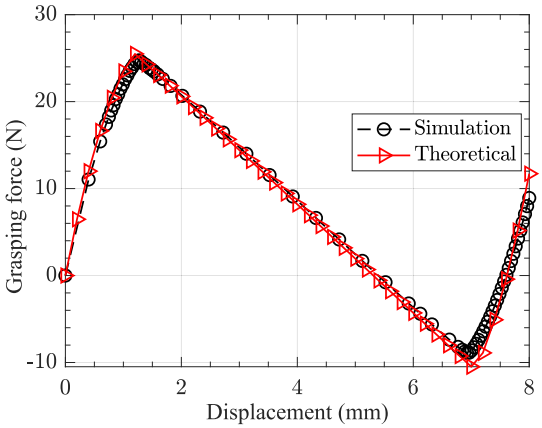

(a) Force-displacement curve

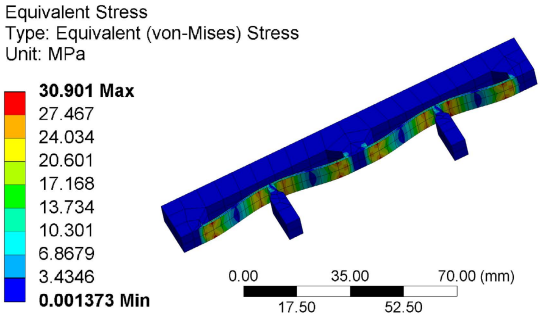

(b) Stress distribution

FIGURE 6. Simulation verification of the BM.

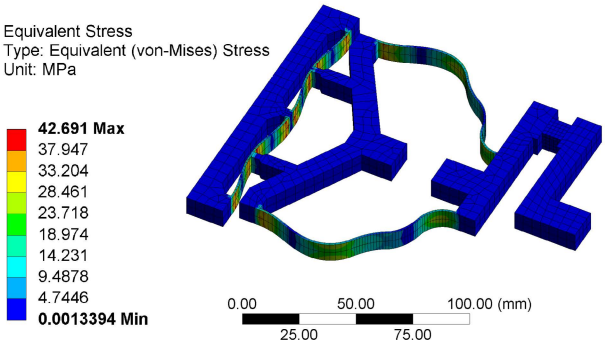

FIGURE 7. FEA model of the gripper.

which coincides with the theoretical value with an error less than 1.33%. The maximum stress, 42.22 MPa, is within the allowable stress range of the material.

The bistable characteristics of the BM is then investigated, as demonstrated in Figure 6. The simulation results coincide with the theoretical value with an error less than 3.3%. The maximum stress is 30.90 MPa,which is within the allowable stress range of the material.

The FEA model of the developed gripper is shown in Figure 7. The force behavior is then simulated during gripping manipulations, as depicted in Figure 8. A stroke of 17.8 mm and 11.9 mm is generated by the gripper in unpreloaded and preloaded status, respectively. It can be seen that simulation results and theoretical results show good consistency, which confirms the performance of the proposed gripper. The discrepancies between the model prediction and the finite element analysis in the present work are mainly contributed by the numerical configurations such as the mesh type and size.

V. EXPERIMENTS

In this section, a prototype is fabricated and tested to verify its performance.

The experimental setup established to measure actual force-displacement curve is illustrated in Figure 9. A prototype of the developed compliant gripper is fabricated through fused deposition modeling (FDM)-based 3D printing technology, of which the dimensions are described in Table 1. The support platform of the prototypes is fixed with the loading

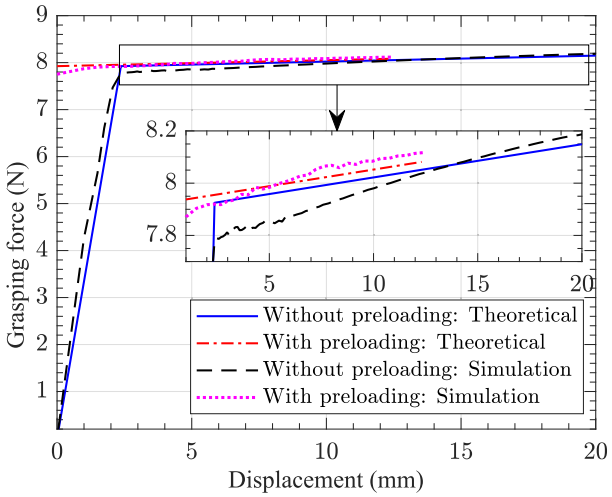

FIGURE 8. Simulation verification of the gripper.

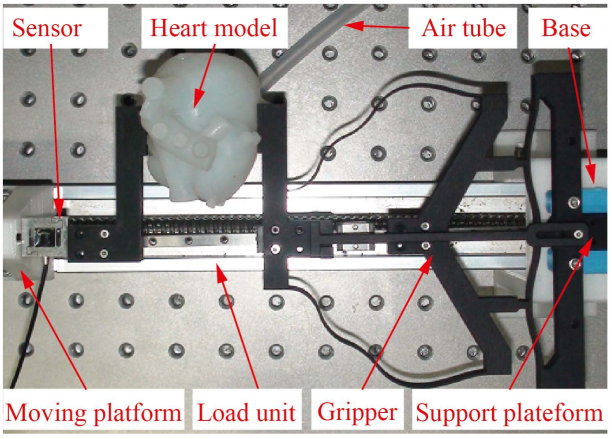

FIGURE 9. Experimental setup of the compliant gripper.

unit and the base by bolts. The force sensor is mounted on the moving platform, which is driven by a stepper motor to incrementally move along its travel direction. The other end of the sensor is in contact with the active jaw of the prototype, where the force data is recorded through a data acquisition card. An air compressor (TYW-500, from Suzhou Tongyi Co. Ltd)and a pressure regulator (SR200, from AirTac International Group) are used to inflate the heart model.

Without losing generality, a silicone heart model is fabricated as the grasping object, of which the overall dimension is 60 mm × 60 mm × 95 mm. Air is periodically inflated to the heart model to simulate the active deformation.

The mechanical behavior of the developed gripper prototype is first investigated using the heart model under different inflating pressures. Before each experiment, the heart model is first inflated to a specified pressure via pressure regulator. Then, adjust the jaws gap along the guide rail to make it slightly larger than the heart model. The left jaw driven by a stepper motor moves along its travel direction, where the reaction force and displacement data were recorded when the

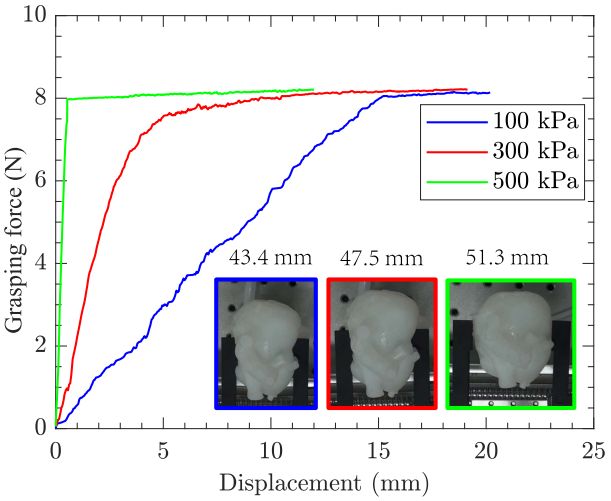

FIGURE 10. Grasping force variation of the heart model with different pressures.

TABLE 2. Measured results of the compliant gripper.

Item	Object size (mm)	Force (N)	Stiffness (N/mm)
1	43.40	8.10	0.0184
2	47.50	8.15	0.0182
3	51.30	8.10	0.0185

jaws were in contact with the heart model. Figure 10 and Table. 2 demonstrate the experimental results of the force-displacement relationships. A constant force of 8.12 N with a stiffness of 0.0184 N/mm is observed under different inflating pressures. The relative error of output force is 0.98 %. The proposed gripper exhibits good robustness to changes in size and stiffness of the objects. As the pressure increases, a smaller input displacement is required before achieving the desired constant force stage. Note that the curve shape is mainly determined by the relative stiffness of the gripper and the heart model. When the stiffness of the heart model is less than that of the gripper, the heart model deforms more easily than gripper, resulting in non-constant force output. When the stiffness of the heart model is larger than that of the gripper, the gripper deforms more easily than the heart model, resulting in constant force output. It is also noting that the stiffness of the heart model (soft material) is affected by its deformation and inflating pressures. At a pressure of 100 kPa and 300 kPa, the initial stiffness of the heart model is less than that of the gripper. As the deformation increases, the stiffness of the heart model increases until it is greater than the stiffness of the gripper. At a pressure of 500 kPa, the initial stiffness of the heart model is larger than that of the gripper, resulting in a constant force output at contact.

The mechanical behavior of the developed gripper prototype is then investigated using the heart model under slowly increasing and periodically inflating pressure. As shown in Figure 11, the grasping force remains almost constant

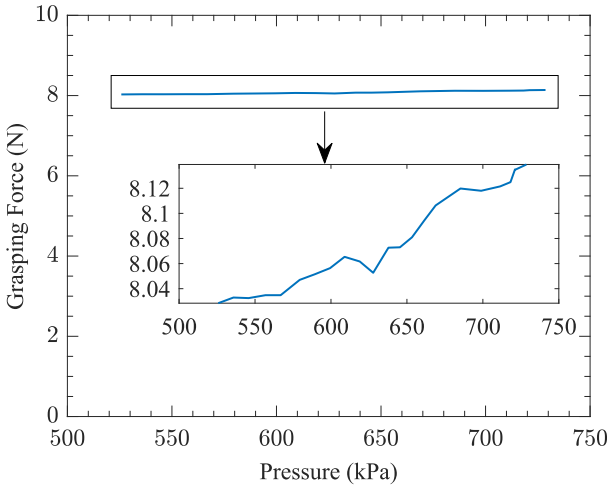

FIGURE 11. Grasping force variation of the heart model under slowly increasing inflating pressure.

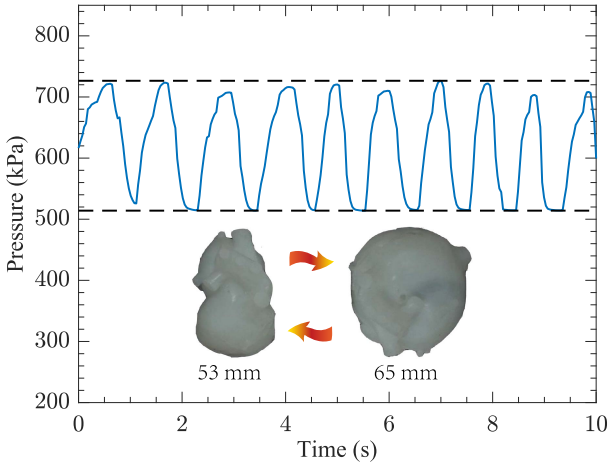

(a) Pressure variation

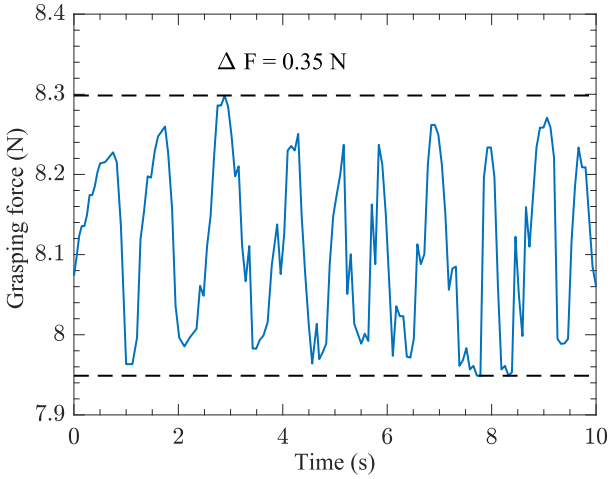

(b) Grasping force variation

FIGURE 12. Grasping force variation of the heart model under periodically inflating pressure.

(8.00 N - 8.06 N) when the inflating pressure increases slowly from 525 kPa - 728 kPa. The maximum fluctuation of the output force is 0.11 N with a relative error of 1.36 %. Further, fluctuate air pressure is inflated to the heart model at a frequency of 1 Hz to simulate heartbeat, Figure 12(a), the dimension of the heart model varies between 53 mm and 65 mm. Figure 12(b) shows the measuring results of grasping force. It is shown that the average output force is 8.11 N, the maximum fluctuation of grasping force is 0.35 N, and the maximum relative error is 4.32 %. The error may come from the nonlinear deformation of the silicone heart model, manufacturing and assembly errors of the prototype. The reader is recommended to watch the supplementary video for more understanding of the grasping process.

Remark 1: This paper focusses on the design, analysis and test of a conceptual gripper that is capable of manipulating actively deformable objects. To focus on the work, a manual gripper is developed as a particular case study, where the jaws compose of a passive constant-force jaw and an active jaw. Due to the large working stroke, direct drive units, such as voice coil motors, can be used to drive the gripper. In this work, the gripper is driven by stepper motor to demonstrate the grasping experiments. Further efforts on miniaturized design and integration with appropriate drive units and multi-DOF motion platform or robot arm are still needed to fulfill practical engineering tasks.

VI. CONCLUSION

In this paper, a constant force compliant gripper for grasping actively deformable objects was developed. The constant force in a large range was obtained by curved-beam compliant mechanism. The non-constant force motion range was eliminated via curved-beam bistable mechanism. According to the CBCM, theoretical models were further established to predict the mechanical behavior of the CFM and BM, for purpose of parameter optimizations. Comprehensive experiments on an additive manufactured prototype were investigated to verify the performance of the developed gripper. Results shows that the maximum fluctuation of grasping force is 0.35 N when the size of the heart model varied periodically between 53 mm and 65 mm at a frequency of 1 Hz, which demonstrates the feasibility of the design of the gripper. We will further explore the application of the proposed gripper to bioengineering manipulation.

CONFLICTS OF INTEREST

The authors declare that they have no conflicts of interest.

REFERENCES

[1] A. H. H. Hosseinabadi and S. E. Salcudean, "Force sensing in robot-assisted keyhole endoscopy: A systematic survey," *Int. J. Robot. Res.*, vol. 41, no. 2, pp. 136–162, Feb. 2022.

[2] T. L. Thomas, V. K. Venkiteswaran, G. K. Ananthasuresh, and S. Misra, "Surgical applications of compliant mechanisms: A review," *J. Mech. Robot.*, vol. 13, no. 2, pp. 1–21, Apr. 2021.

[3] Y. Wei and Q. Xu, "A survey of force-assisted robotic cell microinjection technologies," *IEEE Trans. Autom. Sci. Eng.*, vol. 16, no. 2, pp. 931–945, Apr. 2019.

[4] A. Milojević, S. Linß, Ž. Ćojbašić, and H. Handroos, "A novel simple, adaptive, and versatile soft-robotic compliant two-finger gripper with an inherently gentle touch," *J. Mech. Robot.*, vol. 13, no. 1, p. 379, Feb. 2021.

[5] Z. Lyu and Q. Xu, "Recent design and development of piezoelectric-actuated compliant microgrippers: A review," *Sens. Actuators A, Phys.*, vol. 331, Nov. 2021, Art. no. 113002.
[6] F. Zhong, Y. Wang, Z. Wang, and Y.-H. Liu, "Dual-arm robotic needle insertion with active tissue deformation for autonomous suturing," *IEEE Robot. Autom. Lett.*, vol. 4, no. 3, pp. 2669–2676, Jul. 2019.
[7] J. Huang, Y. Cai, X. Chu, R. H. Taylor, and K. W. S. Au, "Non-fixed contact manipulation control framework for deformable objects with active contact adjustment," *IEEE Robot. Autom. Lett.*, vol. 6, no. 2, pp. 2878–2885, Apr. 2021.
[8] B. Xu and S. Y. Ko, "Novel force sensing module for a concentric tube-based vitreoretinal surgical robot," *Sens. Actuators A, Phys.*, vol. 316, Dec. 2020, Art. no. 112395.
[9] T. Takizawa, T. Kanno, R. Miyazaki, K. Tadano, and K. Kawashima, "Grasping force estimation in robotic forceps using a soft pneumatic actuator with a built-in sensor," *Sens. Actuators A, Phys.*, vol. 271, pp. 124–130, Mar. 2018.
[10] Y. Xie, J. Yu, and H. Zhao, "Deterministic design for a compliant parallel universal joint with constant rotational stiffness," *J. Mech. Robot.*, vol. 10, no. 3, Jun. 2018, Art. no. 031006.
[11] T. Kumar Das, B. Shirinzadeh, A. Al-Jodah, M. Ghafarian, and J. Pinskier, "A novel compliant piezoelectric actuated symmetric microgripper for the parasitic motion compensation," *Mech. Mach. Theory*, vol. 155, Jan. 2021, Art. no. 104069.
[12] S. Permana, E. Grant, G. M. Walker, and J. A. Yoder, "A review of automated microinjection systems for single cells in the embryogenesis stage," *IEEE/ASME Trans. Mechatronics*, vol. 21, no. 5, pp. 2391–2404, Oct. 2016.
[13] T. Ye, J. Ling, X. Kang, Z. Feng, and X. Xiao, "A novel two-stage constant force compliant microgripper," *J. Mech. Des.*, vol. 143, no. 5, May 2021, Art. no. 053302.
[14] G. Hao, J. Mullins, and K. Cronin, "Simplified modelling and development of a bi-directionally adjustable constant-force compliant gripper," *Proc. Inst. Mech. Eng. C, J. Mech. Eng. Sci.*, vol. 231, no. 11, pp. 2110–2123, Jun. 2017.
[15] Y. Wei and Q. Xu, "Design and testing of a new force-sensing cell microinjector based on small-stiffness compliant mechanism," *IEEE/ASME Trans. Mechatronics*, vol. 26, no. 2, pp. 818–829, Apr. 2021.
[16] Y. Miao and J. Zheng, "Optimization design of compliant constant-force mechanism for apple picking actuator," *Comput. Electron. Agricult.*, vol. 170, Mar. 2020, Art. no. 105232.
[17] C.-H. Liu, F.-M. Chung, and Y.-P. Ho, "Topology optimization for design of a 3D-printed constant-force compliant finger," *IEEE/ASME Trans. Mechatronics*, vol. 26, no. 4, pp. 1828–1836, Aug. 2021.
[18] T. Ye, J. Ling, T. Yao, and X. Xiao, "Design of a 2-DOF constant force compliant microgripper for optical switch assembly," in *Proc. 46th Annu. Conf. IEEE Ind. Electron. Soc. (IECON)*, Oct. 2020, pp. 4403–4408.
[19] X. Zhang and Q. Xu, "Design and analysis of a 2-DOF compliant gripper with constant-force flexure mechanism," *J. Micro-Bio Robot.*, vol. 15, no. 1, pp. 31–42, Jun. 2019.
[20] Z. Lyu and Q. Xu, "Design and analysis of a new compliant microgripper with two working modes," in *Proc. IEEE Int. Conf. Manipulation, Manuf. Meas. Nanosc. (3M-NANO)*, Aug. 2021, pp. 65–70.
[21] G. Hao, H. Li, A. Nayak, and S. Caro, "Design of a compliant gripper with multimode jaws," *J. Mech. Robot.*, vol. 10, no. 3, Jun. 2018, Art. no. 031005.
[22] G. Hao and J. Zhu, "Design of a monolithic double-slider based compliant gripper with large displacement and anti-buckling ability," *Micromachines*, vol. 10, no. 10, p. 665, Sep. 2019.
[23] F. Daniel, J. Fontenot, and A. D. Radadia, "Characterization of an electrothermal gripper fabricated via extrusion-based additive manufacturing," *Sens. Actuators A, Phys.*, vol. 333, Jan. 2022, Art. no. 113302.
[24] Q. Zhang, P. Yan, and H. Wang, "A curved-beam based quasi-constant force mechanism supporting large range and force-sensitive robotic manipulation," *Mech. Mach. Theory*, vol. 172, Jun. 2022, Art. no. 104799.
[25] H. Hussein and M. I. Younis, "Analytical study of the snap-through and bistability of beams with arbitrarily initial shape," *J. Mech. Robot., Trans. ASME*, vol. 12, no. 4, Aug. 2020, Art. no. e0168218.
[26] F. Ma and G. Chen, "Modeling large planar deflections of flexible beams in compliant mechanisms using chained beam-constraint-model," *J. Mech. Robot., Trans. ASME*, vol. 8, no. 2, 2016, Art. no. 021018.
[27] S. Awtar and S. Sen, "A generalized constraint model for two-dimensional beam flexures: Nonlinear load-displacement formulation," *J. Mech. Des.*, vol. 132, no. 8, Aug. 2010, Art. no. 081008.
[28] G. Chen, F. Ma, G. Hao, and W. Zhu, "Modeling large deflections of initially curved beams in compliant mechanisms using chained beam constraint model," *J. Mech. Robot.*, vol. 11, no. 1, Feb. 2019, Art. no. 011002.
[29] M. Alturki and R. Burgueño, "Response characterization of multistable shallow domes with cosine-curved profile," *Thin-Walled Struct.*, vol. 140, pp. 74–84, Jul. 2019.

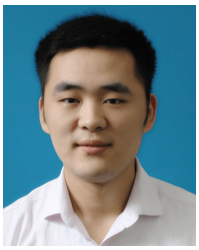

QINGYI ZHANG received the B.E. and M.S. degrees in agricultural engineering from Nanjing Agricultural University, Nanjing, China, in 2014 and 2017, respectively. He is currently pursuing the Ph.D. degree in mechatronics engineering with Shandong University, Jinan, China. His research interests include compliant mechanisms, force-sensitive manipulator design, and modeling and their applications.

PENGBO LIU (Member, IEEE) received the B.E. degree in mechanical engineering from the Ocean University of China, Qingdao, China, in 2012, and the Ph.D. degree in mechatronics engineering from Shandong University, Jinan, China, in 2018. Since 2019, he has been a Lecturer with the School of Mechanical Engineering, Qilu University of Technology (Shandong Academy of Sciences), Jinan. He has published more than 20 scientific articles, and holds six granted/pending patents. His research interests include design, modeling, and control of high-precision mechatronic systems, and nanoscale manipulation and measurement. He was awarded the Best Paper in Theory on IEEE/ASME International Conference on Mechatronic and Embedded Systems and Applications in 2019.

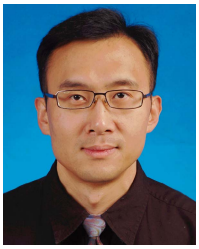

PENG YAN (Senior Member, IEEE) received the B.S. and M.S. degrees in electrical engineering from Southeast University, Nanjing, China, in 1997 and 1999, respectively, and the Ph.D. degree in electrical engineering from The Ohio State University, Columbus, OH, USA, in 2003. He worked in various industry positions, before joining Shandong University, including as a Staff Scientist at the United Technologies Research Center, East Hartford, CT, USA, from 2010 to 2011; and as a Senior Staff Engineer at Seagate Technology, Twin Cities, MN, USA, from 2005 to 2010. He is currently a Full Professor with the School of Mechanical Engineering, Shandong University, Jinan, China. His current research interests include robust control, hybrid systems, and control of high-precision mechatronics.